J|A|C|S
ARTICLES
Published on Web 08/30/2002

Atomistic Models for CeO_2(111), (110), and (100) Nanoparticles, Supported on Yttrium-Stabilized Zirconia

Dean C. Sayle,*,† S. Andrada Maicaneanu,†,§ and Graeme W. Watson‡

Contribution from the Department of Environmental and Ordnance Systems, Cranfield University, Royal Military College of Science, Shrivenham, Swindon, U.K., SN6 8LA, and Department of Chemistry, Trinity College, Dublin 2, Ireland

Received May 6, 2002

Abstract: Ceria is an important component in three-way catalysts for the treatment of automobile exhaust gases owing to its ability to store and release oxygen, a property known as the oxygen storage capacity. Much effort has been focused on increasing the OSC of ceria, and one avenue of exploration is the ability to fabricate CeO_2-based catalysts, which expose reactive surfaces. Here we show how models for a polycrystalline CeO_2 thin film, which expose the (111), (110), and dipolar (100) surfaces, can be synthesized. This is achieved by supporting the CeO_2 thin film on an yttrium-stabilized zirconia substrate using a simulated amorphization and recrystallization strategy. In particular, the methodology generates models which reveal the atomistic structures present on the surface of the reactive faces and provides details of the grain-boundary structures, defects (vacancies, substitutionals, and clustering), and epitaxial relationships. Such models are an important first step in understanding the active sites at the surface of a catalytic material.

Introduction

Ceria is an important component in three-way catalysts for the treatment of automobile exhaust gases[1] because of its ability to store and release oxygen. This property of ceria called the *oxygen storage capacity* (OSC) represents the ability of ceria to shift from Ce^{4+} to Ce^{3+} in reducing atmosphere and from Ce^{3+} to Ce^{4+} under oxidizing conditions with charge compensation facilitated via oxygen vacancies. Accordingly, CO and hydrocarbons can be oxidized simultaneously with the reduction of NO.

Experimental and theoretical studies[1−3] have shown that the reducibility of CeO_2 can be modified via the introduction of dopant cations, such as Zr^{4+}, into the material. The resulting solid solution facilitates a defective fluorite structure with improved oxygen mobility.

An alternative mechanism for enhancing the OSC of ceria is to support a thin film of the material on an oxide substrate. One rationale underlying this strategy is the ability to stabilize reactive CeO_2 surfaces. For example, while the CeO_2(111) surface is the most stable[4,5] and consequently the one which is predominantly exposed, it is also inherently less reactive as compared with the (less stable) CeO_2(110). In particular, the energy required to create oxygen vacancies on the surface of CeO_2(111), which is directly related to the OSC of the material, is greater as compared with that of CeO_2(110).[4] In addition, a theoretical study by Sayle et al.[6] suggested that CeO_2, when supported on Al_2O_3(001), exhibits a lower oxygen formation energy as compared with the unsupported CeO_2. Experimental studies have identified weakly bound surface oxygen species on ceria films deposited on Al_2O_3, which are not present on the unsupported CeO_2(111).[7] Moreover, yttrium-stabilized zirconia (YSZ), when used as a substrate, was found to be more efficient at promoting ceria reducibility than α-Al_2O_3 or polycrystalline zirconia.[7,8] Theoretical studies by Sayle et al. have shown that when supported, the overlying thin film responds structurally to both the lattice misfit associated with the system and the interfacial interactions. This can lead to the evolution of a variety of structural modifications induced into both the thin film and the underlying substrate material and may include dislocations arrays, grain boundaries, point defects (vacancies, interstitials, and substitutionals), low interfacial ion densities, lattice slip, epitaxial configurations, and associated relaxation of the lattices resulting in local and global changes in geometry (bond distances).[9−11] Clearly, within a material with catalytic properties, these types of structural features can influence positively the catalytic properties of the material. For example, grain boundaries facilitate the exposure of less stable surfaces and encourage oxygen ion migration and exchange near

* To whom correspondence should be addressed. E-mail: sayle@rmcs.cranfield.ac.uk.
† Cranfield University.
‡ Trinity College.
§ Current address: Department of Chemical Technology, "Babes-Bolyai" University, Arany Janos St., No. 11, 3400 Cluj-Napoca, Romania.

(1) Trovarelli, A. *Catal. Rev.-Sci. Eng.* **1996**, *38*, 439.
(2) Balducci, G.; Kašpar, J.; Fornasiero, P.; Graziani, M.; Islam, M. S.; Gale, J. D. *J. Phys. Chem. B* **1997**, *101*, 1750.
(3) Kašpar, J.; Fornasiero, P.; Graziani, M. *Catal. Today* **1999**, *50*, 285.
(4) Sayle, T. X. T.; Parker, S. C.; Catlow, C. R. A. *Surf. Sci.* **1994**, *316*, 329.
(5) Nörenberg, H.; Harding, J. H. *Surf. Sci.* **2001**, *477*, 17.
(6) Sayle, D. C.; Sayle, T. X. T.; Parker, S. C.; Harding, J. H.; Catlow, C. R. A. *Surf. Sci.* **1995**, *334*, 170.
(7) Putna, E. S.; Vohs, J. M.; Gorte, R. J. *J. Phys. Chem.* **1996**, *100*, 17862.
(8) Putna, E. S.; Bunluesin, T.; Fan, X. L.; Gorte, R. J.; Vohs, J. M.; Lakis, R. E.; Egami, T. *Catal. Today* **1999**, *50*, 343.
(9) Sayle, D. C. *J. Mater. Chem.* **1999**, *9*, 2961.
(10) Sayle, D. C.; Watson, G. W. *J. Mater. Chem.* **2000**, *10*, 2241.
(11) Sayle, D. C.; Watson, G. W. *Surf. Sci.* **2001**, *473*, 97.

the surface, increasing the OSC.[12] Grain boundaries in CeO_2 systems were identified by Vallet-Regi et al.[13] using spray pyrolysis and by Španková et al.[14] for ceria films deposited on sapphire. It was also found that the ceria pyrosol spheres and the ceria thin films exhibit (111) and (100) oriented crystallites, which are distributed randomly. In addition, a simulation study by Baudin et al. suggests that when CeO_2 is supported on α-Al_2O_3(0001), the mean square displacements of ions at the interfacial region increase 2−3 times as compared with the component CeO_2 and α-Al_2O_3 slabs.[15]

Supporting a thin film on a substrate material can thus be associated with two roles, which may help improve the catalytic properties of the materials: first, to facilitate the exposure of potentially reactive surfaces, which may not be possible if unsupported and, second, to introduce structural modifications into the supported thin film, which leads to an increased lability and mobility of surface oxygen species. The reduction of ceria is also facilitated by contact between ceria and a precious metal such as Rh and Pt[1,16] in the presence of a reducing agent (CO, H_2, or hydrocarbons). It has also been shown that the OSC can be improved by thermal treatment of the catalyst.[1]

In a previous study, we employed simulation techniques to explore the structure of CeO_2 thin films supported on a YSZ-(111) substrate. The resulting CeO_2 exposed the CeO_2(111) at the interface and surface and comprised a variety of structural modifications,[17] including misfit dislocation arrays with periodicities in accord with experiment. In this present study, we extend our previous work to explore the influence of supporting a CeO_2 thin film on a YSZ(110) substrate. The aim is to facilitate exposure of the more reactive CeO_2(110) surface to help further our understanding of surface active sites and to induce structural modifications into the supported thin film, which may help improve the catalytic properties of the material. Because it has been shown that by supporting CeO_2 on a substrate material the catalytic properties may be enhanced, elucidating the structural features, which evolve upon supporting the material, will have important implications for catalytic systems.

We consider in this study the CeO_2/YSZ(110) system with a level of yttrium doping equal to 9.24 mol % Y_2O_3, which enables high ionic conductivity[18,19] and stability of the zirconia cubic phase at low temperatures.[20]

Methodology

In this section, the potential models used in the study are presented together with a description of the simulation code, followed by a discussion of the amorphization and recrystallization strategy employed to generate models for ceria thin films on a YSZ(110) substrate.

Potential Models. The calculations presented in this study are based on the Born model for ionic solids, with potential parameters taken from Lewis and Catlow[21] for Y^{3+}, Dwivedi and Cormack[22] for Zr^{4+} and O^{2-} ions, and Sayle et al.[4] for Ce^{4+}. These potentials have been employed to model lattice parameters,[23] thermal expansivities,[24] conductivity, and diffusion properties[24] for CeO_2-ZrO_2, $ZrO_2-M_xO_y$, and $CeO_2-M_xO_y$ solid solutions in accord with experiment.

The dynamical simulations, which employ three-dimensional periodicity, were performed using the DL_POLY code,[25] and therefore a void, 60 Å in size, normal to the surface was introduced to represent the free surface. The simulation cell contains ions distributed in two regions:[26] region I comprises the thin film and the first six repeat units of the support, and ions within this region are allowed to move under dynamical simulation, while region II comprises ions (four repeat units of the support) that are kept fixed to ensure the correct crystalline environment.

In addition, a mean field strategy[27] was employed to represent the fixed ions comprising the yttrium-stabilized zirconia support in region II. The $Zr_xY_{1-x}O_{2-x/2}$ representing the region II of the support is assumed to contain a single, "hybrid" cationic species between Zr^{4+} and Y^{3+} (10% of the zirconium ions are replaced with yttrium). Accordingly, the short-range potential parameters describing all of the interactions involving the new "hybrid" species can be calculated.[27] This strategy is discussed in more detail elsewhere.[17]

In this study, models for the CeO_2/YSZ(110) system are generated using a simulated amorphization and recrystallization strategy,[9,11] which was employed successfully in a previous study on the CeO_2/YSZ(111) system.[17] Essentially, the method entails a controlled amorphization of the thin film followed by recrystallization. When amorphous, the ions comprising the ceria thin film have high ionic mobility and therefore are able to rearrange into a low-energy configuration within the (limited) time scales accessible to typical dynamical simulations. To induce amorphization, the thin film is constrained initially under considerable compression and placed on top of the support. The thin film responds, under dynamical simulation, to the huge initial pressure of this configuration and relieves it via a transition from a crystalline to an amorphous structure. Prolonged dynamical simulation results in the recrystallization of the thin film together with the evolution of structural modifications as the system responds to the lattice misfit and interaction potential of the support.

Construction of the Model. To generate the CeO_2/YSZ(110) interface, four CeO_2(110) repeat units (thick) were placed directly on top of 10 repeat units of a 40 × 20 ZrO_2(110) support (six repeat units included in region I and four repeat units included in region II), using a "cube-on-cube" methodology.[28] The "40 × 20" corresponds to 40 and 20 zirconium ions along each side of the simulation cell, which results in a surface area of 14 573 Å^2 and comprises 41 496 ions. The CeO_2 was then compressed by 31%. The compression imposed upon the CeO_2 is quite critical to the success of the amorphization and recrystallization strategy. If it is much lower than 31% (i.e., 20%), then the thin film fails to recrystallize, and the thin film, after recrystallization, remains amorphous. Conversely, if the compression is too high, the simulation fails catastrophically,[29] owing to the considerable velocity of the ions under dynamical simulation.

The second step was to introduce the mean field "hybrid" ions into region II of the support (effectively changing the ZrO_2 support into

(12) Dmowski, W.; Mamontov, E.; Egami, T.; Putna, S.; Gorte, R. *Physica B* **1998**, *248*, 95.
(13) Vallet-Regi, M.; Conde, F.; Nicolopoulus, S.; Ragel, C. V.; Gonzáles-Calbet, J. M. *Mater. Sci. Forum* **1997**, *235*, 291.
(14) Španková, M.; Vávra, I.; Gaži, Š.; Machajdík, D.; Chromik, Š.; Fröhlich, K.; Hellemans, L.; Beňačka, Š. *J. Cryst. Growth* **2000**, *218*, 287.
(15) Baudin, M.; Wójcik, M; Hermansson, K. *Thin Solid Films* **2001**, *401*, 159.
(16) Trovarelli, A.; de Leitenburg, C.; Boaro, M.; Dolcetti, G. *Catal. Today* **1999**, *50*, 353.
(17) Maicaneanu, S. A.; Sayle, D. C.; Watson, G. W. *J. Phys. Chem. B* **2001**, *105*, 12481.
(18) Brinkman, H. W.; Briels, W. J.; Verweij, H. *Chem. Phys. Lett.* **1995**, *247*, 386.
(19) Yamamura, Y.; Kawasaki, S.; Sakai, H. *Solid State Ionics* **1999**, *126*, 181.
(20) Li, P.; Chen, I.-W.; Penner-Hahn, J. E. *J. Am. Ceram. Soc.* **1994**, *77*, 118.
(21) Lewis, G. V.; Catlow, C. R. A. *J. Phys. C: Solid State Phys.* **1985**, *18*, 1149.
(22) Dwivedi, A.; Cormack, A. N. *Philos. Mag. A* **1990**, *61*, 1.
(23) Balducci, G.; Islam, M. S.; Kašpar, J.; Fornasiero, P.; Graziani, M. *Chem. Mater.* **2000**, *12*, 677.
(24) Khan, M. S.; Islam, M. S.; Bates, D. R. *J. Mater. Chem.* **1998**, *8*, 2299.
(25) Smith, W.; Forester, T. R. The DL_POLY Molecular Simulation Package, URL: http://www.dl.ac.uk/TCSC/Software/DL_POLY.
(26) Watson, G. W.; Kelsey, E. T.; de Leeuw, N. H.; Harris, D. J.; Parker, S. C. *J. Chem. Soc., Faraday Trans.* **1996**, *92*, 433.
(27) Morris, B. C.; Flavell, W. R.; Mackrodt, W. C.; Morris, M. A. *J. Mater. Chem.* **1993**, *3*, 1007.
(28) Sayle, D. C.; Catlow, C. R. A.; Harding, J. H.; Healy, M. J. F.; Maicaneanu, S. A.; Parker, S. C.; Slater, B.; Watson, G. W. *J. Mater. Chem.* **2000**, *10*, 1315.
(29) Sayle, D. C.; Catlow, C. R. A.; Dulamita, N.; Healy, M. J. F.; Maicaneanu, S. A.; Slater, B.; Watson, G. W. *Mol. Simul.* **2002**, *28*, 683.

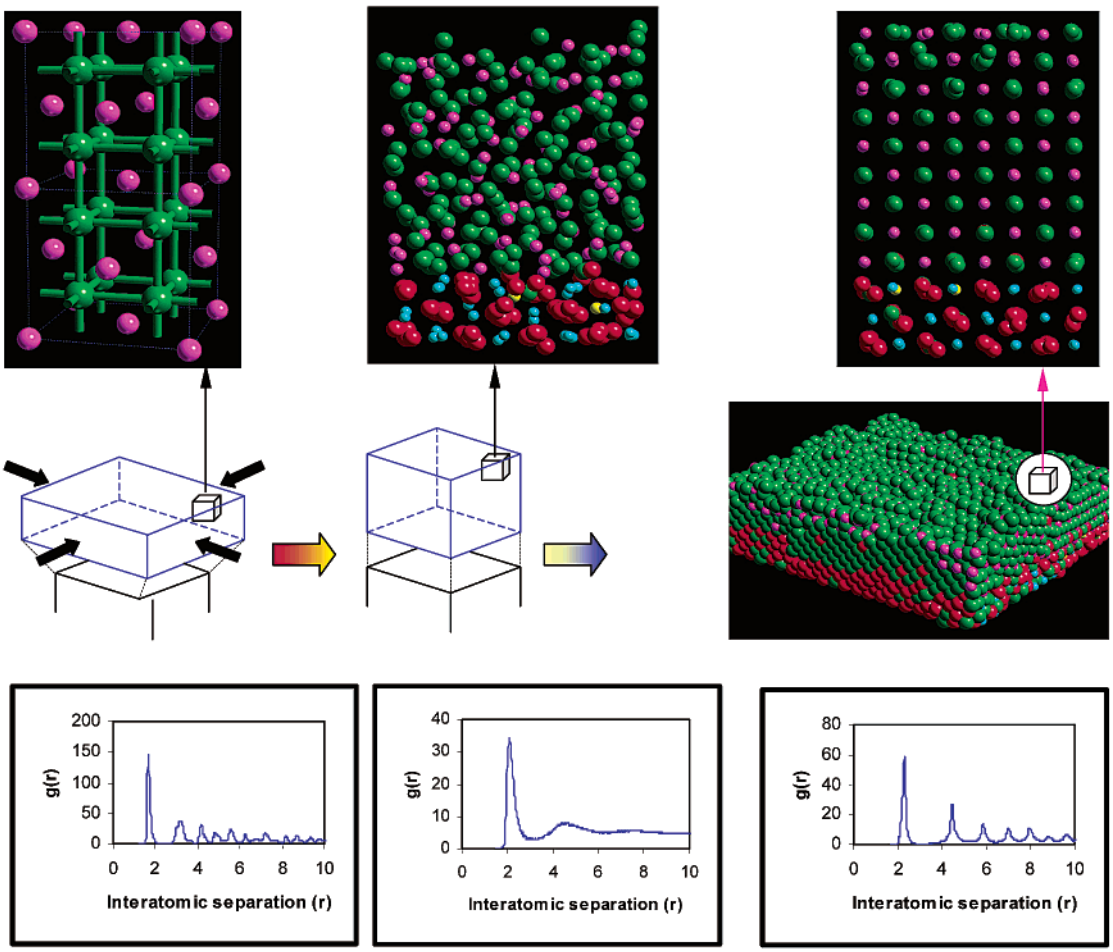

Figure 1. Schematic illustrating the amorphization and recrystallization strategy as applied to the CeO_2/YSZ(110) system. At the top left of the figure, the starting configuration is shown with the CeO_2 adopting its natural fluorite-type structure. Top middle depicts the system after the application of dynamical simulation, which results in an amorphous structural transition. Top right shows the atom positions of part of the CeO_2 thin film at the end of the simulation and shows that the CeO_2 has recrystallized into the fluorite structure. The figures along the middle (left to right) illustrate the initial compression imposed upon the CeO_2 to effect the amorphous transition, the relaxation of the ions comprising the CeO_2 in a direction normal to the interfacial plane as the system attempts to remove the high compressive strain, and the final structure of the simulation cell. At the bottom of the figure, the corresponding Ce−O radial distribution functions for the starting configuration (after 0.005 ps of dynamical simulation), the amorphous structure (0.25 ps), and the final structure are shown with interatomic separations measured in angstroms. Cerium is colored pink, oxygen (CeO_2) is green, oxygen (YSZ) is red, zirconia is blue, and yttrium is yellow.

YSZ) and to scale the entire simulation cell to the new lattice parameter. Specifically, the cell was scaled on the basis of the relative lattice parameters for the parent ZrO_2 (5.057 Å) and the YSZ (5.106 Å). The latter was calculated using the GULP code.[30] Accordingly, the interfacial area increases to 14 749 $Å^2$.

Finally, yttrium species were introduced into region I by replacing 10% of the Zr^{4+} ions with Y^{3+} (480 yttrium ions), corresponding to 9.24 mol % Y_2O_3. Next, 240 oxygen ions were removed to maintain charge neutrality of the system. The MDPREP program[31] was used to introduce yttrium ions and oxygen vacancies at random into the zirconia lattice. The whole simulation cell comprises finally 41 256 ions.

Dynamical simulation, with a time step of 5×10^{-3} ps, was then applied to the system for 325 ps at 2500 K, 155 ps at 2000 K, 85 ps at 1500 K, 20 ps at 1000 K, 85 ps at 500 K, and 260 ps at 0 K; the later acts effectively as an energy minimization. For each temperature, the dynamical simulation was performed until the system was no longer evolving structurally nor energetically.

All simulations were performed within the NVE ensemble: constant number of particles, constant volume, and constant energy with instantaneous velocity scaling to the simulation temperature used throughout. This prevents the large buildup of kinetic energy as the thin film evolves from the highly strained initial configuration, via an amorphous transition, to a crystalline phase with reduced strain and a range of defects.

(30) Gale, J. D. *J. Chem. Soc., Faraday Trans.* **1997**, *93*, 629.
(31) Watson, G. W. MDPREP, A Computer Program for the Preparation and Analysis of Molecular Dynamics Simulations, 2002.

Results

Amorphization and Recrystallization. Figure 1 shows a schematic illustrating the simulated amorphization and recrystallization strategy as applied to the CeO_2/YSZ(110) system. The procedure was also followed by calculating the Ce−O radial distribution functions (RDF) for the supported CeO_2 thin film. These are presented after 0.005 ps, 0.25 ps, and at the end of the simulation at the bottom of Figure 1.

After 0.005 ps, the RDF shows peaks at 1.9, 3.2, and 4.2 Å, which correspond to the parent CeO_2 (thin film) under 31% compression. After 0.25 ps, the CeO_2 thin film loses long-range order, indicating the amorphous transition. During the prolonged dynamical simulation, the thin film starts to regain long-range order after about 150 ps (RDF not shown), indicating recrystallization of the thin film. Finally, at the end of the simulation, the RDF exhibits sharp peaks, indicating a crystalline structure.

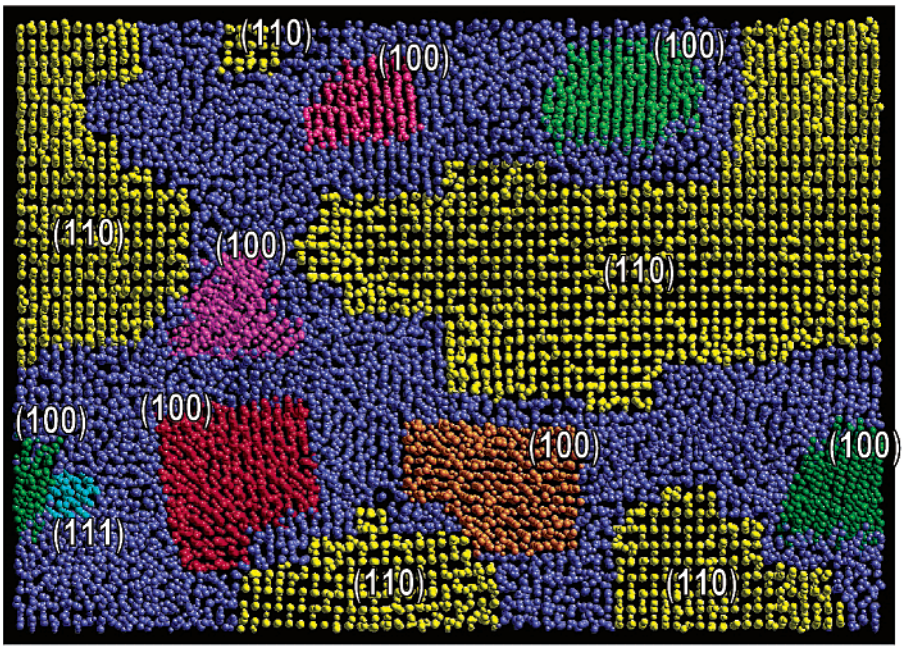

Figure 2. Graphical representation of the atom positions comprising the final CeO_2/YSZ(110) system (plan view). The various misoriented nanocrystallites are colored to aid interpretation of the structure. Indices of the planes exposed at the surface by the various misaligned CeO_2 nanocrystallites are also indicated on the figure.

However, it is clear that the structure has rearranged significantly as shown by a shift of the RDF peaks to 2.3, 4.5, and 5.9 Å, by comparison with the initial strained structure.

Structural Characterization. During the amorphization process, the CeO_2 thin film expands along the surface normal, transforming structurally from four CeO_2 repeat units within the preparatory configuration to nine CeO_2 repeat units with a final thickness of approximately 40 Å. The final CeO_2 thin film has a polycrystalline structure with incomplete surface layers (layers eight and nine), which comprise clusters and isolated CeO_2 groups. In Figure 2, a plan view of the final structure of the CeO_2/YSZ(110) system is presented; a perspective view of the system is shown in Figure 3, which depicts more clearly the surface topography and low coordinative saturation of the surface species.

Inspection of the final structure, Figure 2, reveals that the CeO_2 thin film comprises various nanocrystallites. Surprisingly, the CeO_2 does not expose wholly the CeO_2(110) surface at the interfacial and surface planes, that is, CeO_2(110)/YSZ(110); rather, nanocrystallites exposing CeO_2(111), CeO_2(110), and CeO_2(100) are observed. These are enlarged to aid interpretation in Figure 4a−c, respectively. Moreover, the nanocrystallites, which range from about 50 to 3500 $Å^2$ in area, are also misoriented by various angles and are separated by regions of CeO_2, which appear amorphous (regions colored blue in Figure 2). The exposure of the CeO_2(100) surface is somewhat surprising because this surface is dipolar and less stable as compared with either CeO_2(110) or especially CeO_2(111).[4] Conversely, it is also the most important because it is likely to be the most reactive.

Inspection of Figure 3, using graphical techniques (simple observation of the image is difficult), reveals a surface roughness of about 2−6 Å. One can observe that the CeO_2 thin film exposes the (111) plane, which lies parallel with the interfacial plane (region "1" in the figure). In region "2", there appears a pyramidal shaped hillock, which exposes (111) surfaces at each face with a peak-trough distance, calculated perpendicular to the surface, of about 6 Å. In addition, (110) and (100) surfaces are expressed (regions "3" and "4", respectively). It appears that the surface has facetted, rather than existing simply as a termination of the bulk. Similar behavior has been observed in MgO.[32]

Experimentally, Wang et al., who explored the structure of epitaxial CeO_2 grown by metal-organic chemical vapor deposition at 540 °C on YSZ substrates,[33] determined that the root-mean-square roughness of the CeO_2 films is approximately 4.3 Å, in accord with this study. Close inspection of the CeO_2 grain particles revealed "tetragonal-pyramidal shaped hillocks", which the authors suggested expressed (111) planes.

In Figure 5, the Ce and Zr ion densities, as a function of distance normal to the interfacial plane, are presented for the CeO_2/YSZ(110) system. The ion densities have been calculated using the MDPREP code[31] to indicate any changes in the layers of the fluorite structured lattices. The ion density, $z(x)$, is defined as the number of atoms of a given type, within a range of perpendicular positions in the simulation cell and normalized to the average density:

$$z(x) = \frac{V}{N}\frac{1}{A\delta x}\left\langle \sum_i \delta(x - x_i) \right\rangle \qquad (1)$$

where V is the simulation cell volume, N is the number of atoms of the given type, A is the area of the interface, x_i is the perpendicular height of atom i, and δx is the histogram width over which the δ function gives one. A value of 1.0 thus represents the average density for that species within the entire simulation cell (including the vacuum), with larger values indicating increased density and the formation of well-defined crystal planes.

(32) Watson, G. W.; Kelsey, E. T.; de Leeuw, N. H.; Harris, D. J.; Parker, S. C. *J. Chem. Soc., Faraday Trans.* **1996**, *92*, 433.
(33) Wang, A.; Belot, J. A.; Marks, T. J.; Markworth, P. R.; Chang, R. P. H.; Chudzik, M. P.; Kannewurf, C. R. *Physica C* **1999**, *320*, 154.

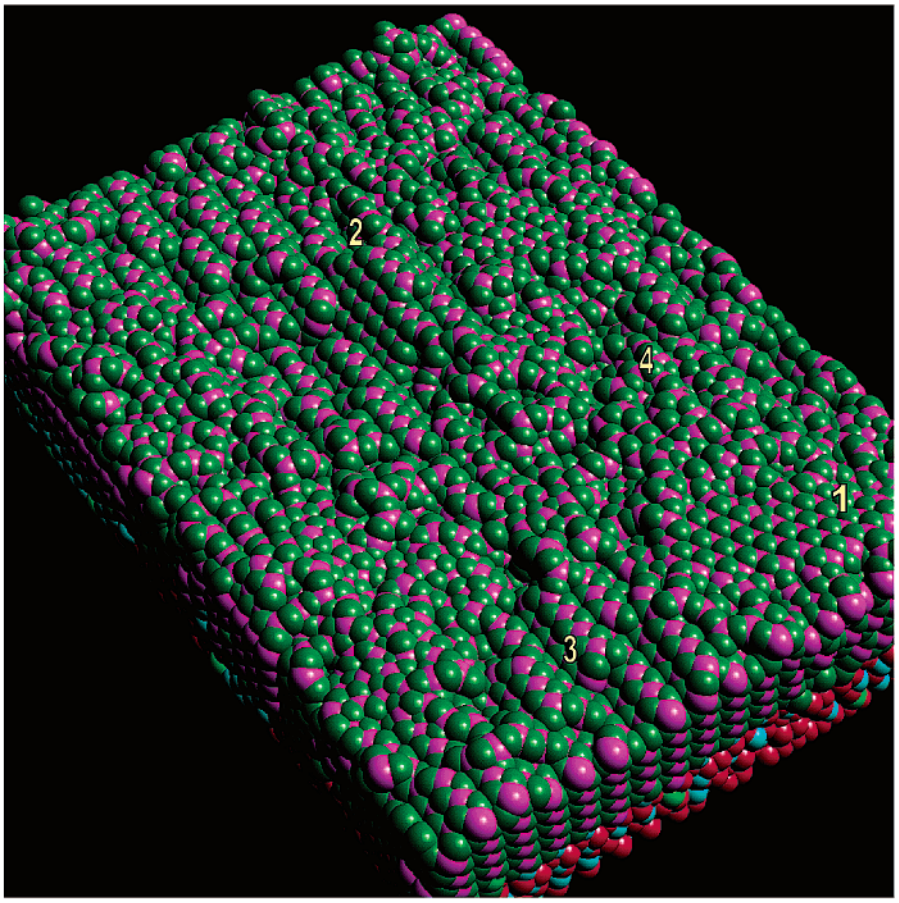

Figure 3. Sphere model representation with perspective of the surface of the CeO_2/YSZ(110) thin film depicting the surface roughness and low coordinative saturation of the surface ions. Color notation is as in Figure 1.

The first six (blue) peaks in Figure 5, located at a depth from −30 to −20 Å, correspond to Zr ions within region I of the simulation cell and reflect the YSZ(110) substrate directly below the overlying CeO_2 thin film. The remaining 8−9 peaks, colored red, correspond to Ce ions within the CeO_2 nanocrystallites. One can observe from the blue trace in Figure 5 that as one approaches the interfacial plane (located at a depth of about −20 Å), the Zr peaks broaden, indicating increased ionic relaxation at the near interface region. Moreover, the trace does not return to zero for the three Zr peaks nearest to the interface. Specifically, within the interfacial region, there is considerable structural disorder as the ions relax to maximize favorable interactions across the interfacial planes. For the overlying CeO_2 thin film, the peaks are well resolved and sharp. This is somewhat surprising because the thin film appears structurally (Figures 2 and 4) to comprise crystalline nanoparticles, interconnected by amorphous regions. One would expect therefore to observe broad peaks with poor if not intractable resolution corresponding to the amorphous regions. Conversely, the presence of sharp peaks indicates a thin film, which exhibits well-defined layers.

To help rationalize the apparently contradictory evidence presented by Figures 2 and 5, that is, whether the regions connecting the nanocrystallites are amorphous or crystalline, graphical techniques were employed to cut parallel with the interfacial plane, a thin slice through the CeO_2 thin film. The Ce and O sublattices, comprising the slice, are presented as plan views in Figure 6a and b, respectively. In addition, small segments (regions 1, 2, and 3 in Figure 6a) are shown in Figure 7a−c, respectively. From Figures 6 and 7, it is apparent that the nanocrystallites, comprising the CeO_2 thin film, are not interconnected by amorphous regions; rather, a complex network of grain boundaries and grain junctions exists, which demonstrates localized disorder.

Clearly, Figure 2 gives the erroneous impression that amorphous regions exist within the CeO_2 thin film. This can be rationalized in that the CeO_2 thin film comprises various *misoriented* nanoparticles interconnected by a complex grain-boundary structure. If one then inspects a two-dimensional (rather than 3D) representation of the film (as portrayed in Figure 2), certain regions are necessarily misaligned to the viewing angle, giving the impression of amorphicity. Grain-boundary and grain-junction disorder, particularly with respect to the oxygen sublattice, compound this difficulty in interpretation.

This section exemplifies the fact that the molecular graphical techniques employed are not solely to provide a flavor of the various structures; rather, they are very powerful analytical tools in rationalizing the atomistic structure of such systems, and consequently they form a major component of such a study.

In contrast to a previous study on the CeO_2(111)/YSZ(111) system, no dislocations within the CeO_2 nanocrystallites were identified to have evolved. We suggest that the polycrystalline structure facilitates increased relaxational freedom at the plethora of grain boundaries and grain junctions, which enables any

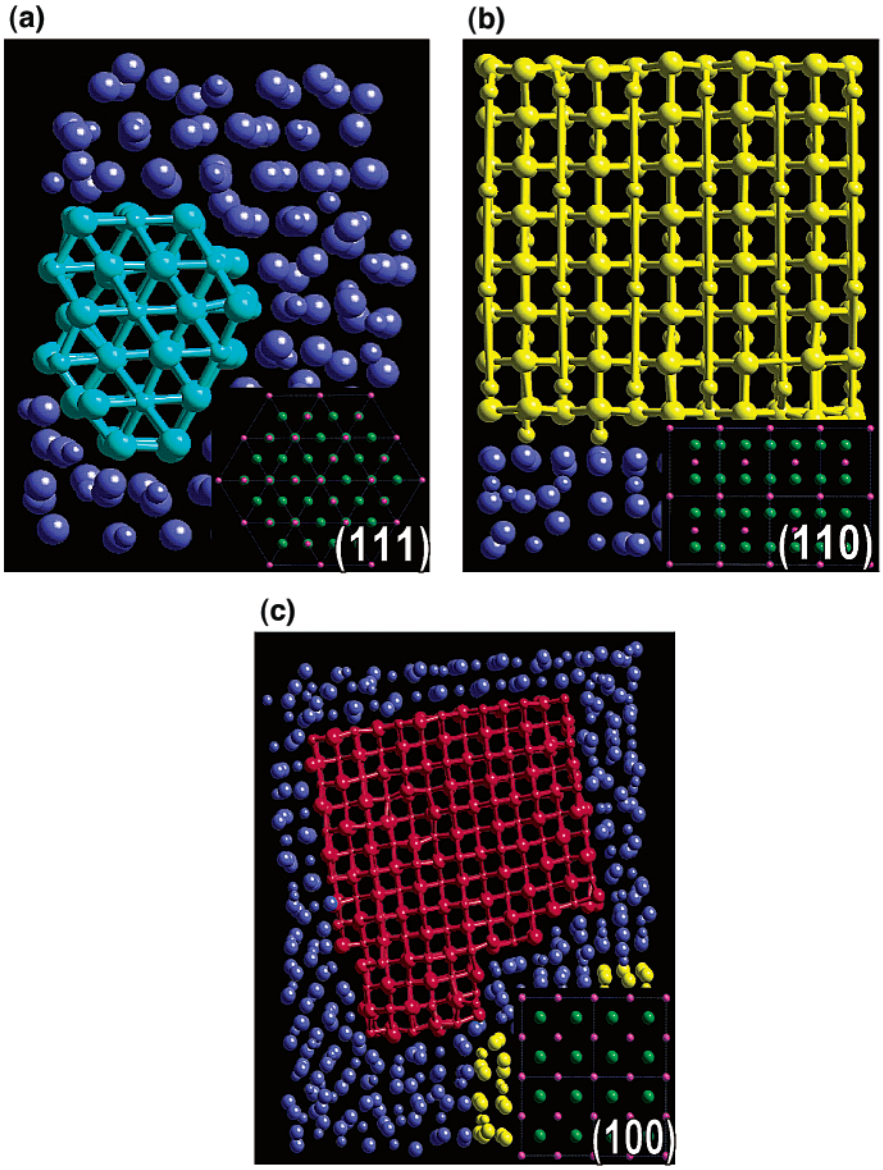

Figure 4. Molecular graphical representations of the various nanocrystallites observed within the CeO_2/YSZ(110) system (Figure 2): (a) CeO_2(111); (b) CeO_2(110); (c) CeO_2(100). The inset at the bottom right-hand corner of each figure shows the crystalline structure corresponding to the perfect fluorite lattice for comparison. To improve clarity of the figures, the underlying YSZ(110) substrate is not shown.

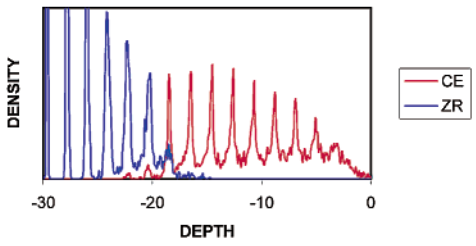

Figure 5. Cerium (red) and zirconium (blue) ion densities, calculated as a function of distance (in angstroms) normal to the interfacial plane within the CeO_2/YSZ(110) system. The ionic densities were integrated over a distance of 0.1 Å. The surface of the CeO_2 thin film is located at a depth of zero.

residual strain within the lattice to be quenched without requiring the evolution of dislocations.

Experimental studies of CeO_2 obtained by spray pyrolysis[13] and r. f. sputtering[14] revealed the presence of polycrystalline CeO_2 particles and surfaces. Ceria particles obtained using spray pyrolysis contain crystallites, randomly distributed, exposing both CeO_2(111) and CeO_2(100) surfaces in accord with this present study. For ceria deposited on a sapphire substrate (r. f. sputtering), the as-deposited CeO_2 layers comprise small mosaic blocks (about 200 Å in size), which are twisted with respect to each other by an angle of 6−7°; (111) and (100) oriented grains can be obtained at 640−680°. In accord with experiment, the simulated models presented in this study can also be seen to have rotated by angles of about 5−10° (for example, Figure 4c).

Defects. A layer-by-layer analysis, using molecular graphical techniques, of the CeO_2 thin film and YSZ support indicates the presence of vacancies: approximately 10% of the Ce and 4% of the Zr lattice sites are vacant and exist predominantly as vacancy clusters. These calculated defect concentrations, which are determined by inspection of the various slices, are necessarily approximate owing to structural perturbations arising from the various grain boundaries within the thin film. In addition, 12% of the cerium lattice sites (thin film) are occupied by zirconium and yttrium, with 7% of the zirconium/yttrium lattice sites in

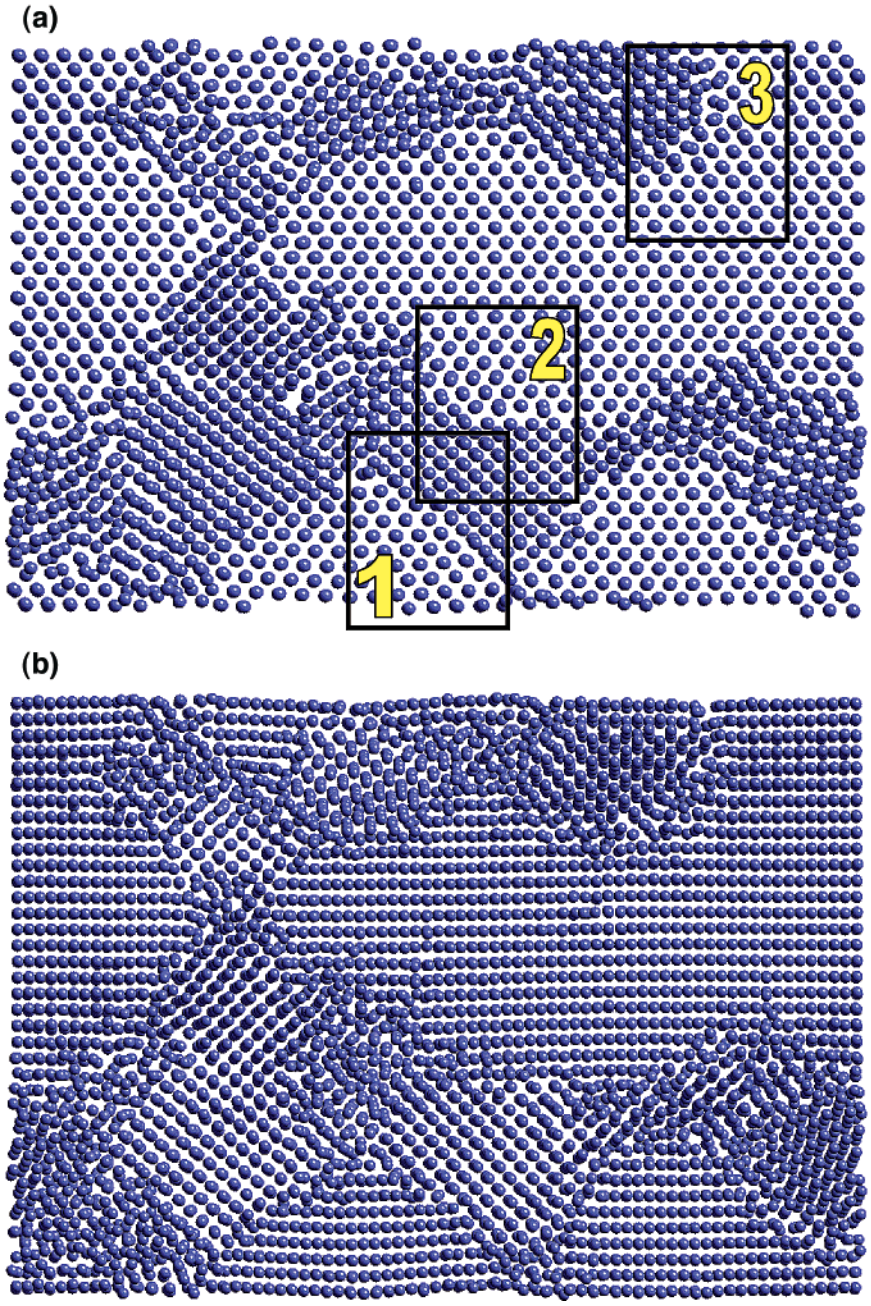

Figure 6. Sphere model representations of the atom positions within a thin slice cut parallel with the interfacial plane through the CeO_2 thin film: (a) Ce sublattice; (b) oxygen sublattice. The slice is 10 Å thick and cut at a depth of −7 to −17 Å (see Figure 5) from the surface of the CeO_2 thin film.

the underlying substrate occupied by cerium. Specifically, one can observe (Figure 5) that the blue trace, which corresponds to Zr ions, extends as far as the third CeO_2 plane. Moreover, underlying the first red peak (CeO_2 interfacial plane), there is a blue peak, which indicates that the Zr ions migrate across the interfacial plane and occupy Ce lattice positions within the interfacial region. The Ce ions displaced can be adjudged to have migrated into the substrate and occupy Zr lattice positions within the two interfacial ZrO_2 planes.

Elucidation of the final structure using graphical techniques reveals that the first five planes of the underlying YSZ support exhibit structural changes. This is in contrast to a previous study on the CeO_2(111)/YSZ(111) system,[17] in which only the first two layers of the substrate were observed to be defective; the CeO_2 comprised also a single crystal. We suggest that the polycrystalline CeO_2 thin film, in which the various nanocrystallites comprising the thin film expose (111), (110), and (100) surfaces at both the interfacial plane and the surface, perturbs the underlying YSZ more strongly than a wholly (111) oriented single crystal.

Limitations associated with the simulations dictate that any relaxation or atomistic disorder cannot be observed further than the first six Zr layers (Figure 5) because ions within this region (region II) are held fixed. While it is conceivable that the disorder might extend further than this, one can observe from Figure 5 that the peaks become sharper as one traverses the substrate (i.e., depth from −20 to −30). Indeed, the resolution of the peak corresponding to Zr ions located at the bottom of region I is almost perfectly sharp, indicating convergence with respect to region size.

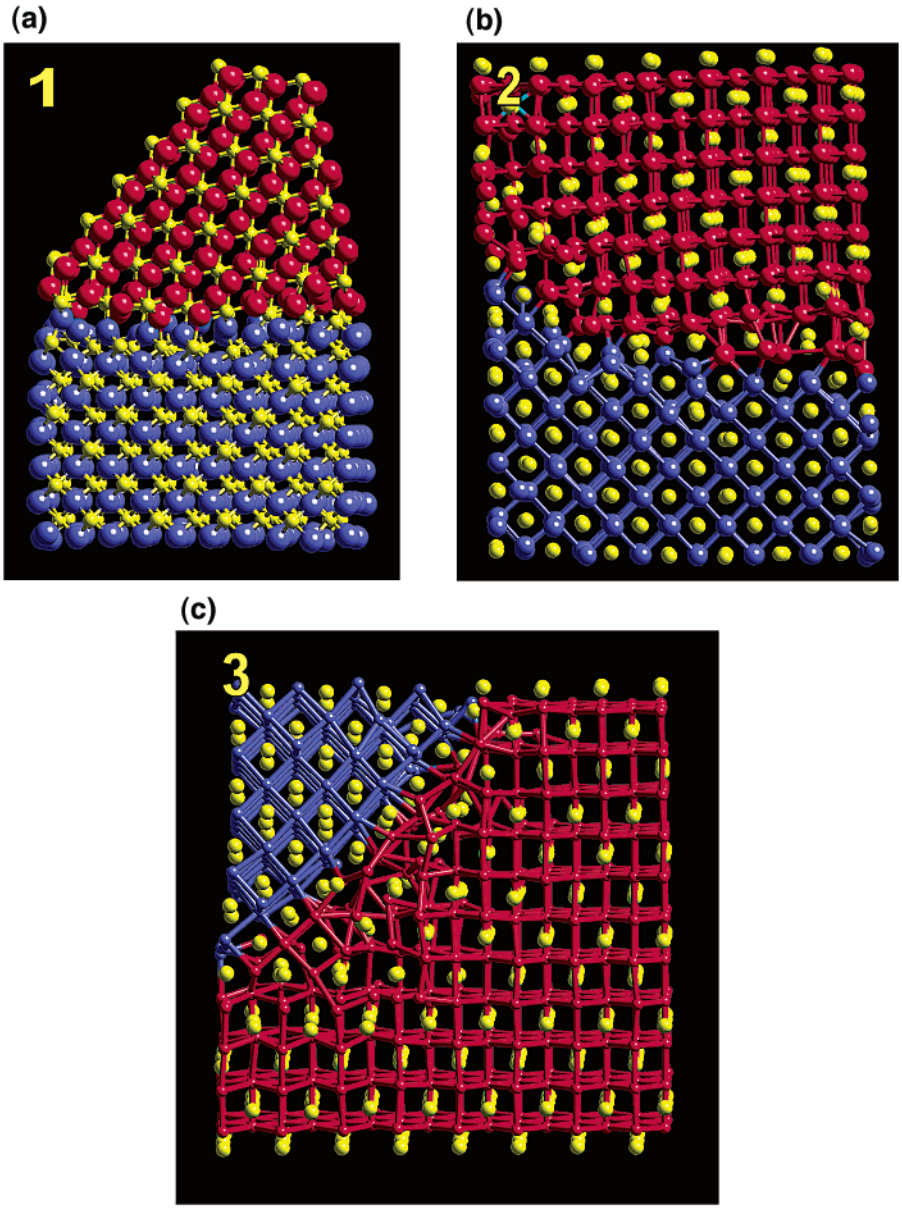

Figure 7. Ball-and-stick model representations of segments (indicated in Figure 6a) of the CeO_2 thin film depicting the grain-boundary structures, which separate the various misoriented CeO_2 nanoparticles comprising the thin film. Parts a, b, and c correspond to regions "1", "2", and "3", respectively, of Figure 6a. Cerium is colored yellow, and oxygen is colored blue and red, the latter to indicate more clearly the positions of the grain-boundary planes.

Epitaxial Considerations. In Figure 8, the Ce sublattice (Figure 6a) is shown in plan view overlaying the cation (Zr, Y) sublattice of an equivalent slice cut through the underlying YSZ substrate. One can observe from this figure that in certain regions, the CeO_2 lies aligned with respect to the underlying YSZ. These regions are then separated by regions of CeO_2, which fall out of alignment. For example, the area enclosed by the blue line comprises a region in which the CeO_2(110) overlies the YSZ(110). If one then traverses from position "1" in the figure, a region where the two lattices are aligned (coincident), to position "2" where the sublattices again become coincident, one can adjudge that there are 16 spacings between the Ce ions and 17 spacings between the underlying zirconium ions; the periodicity for atomic stacking dislocations is calculated to be about 56 Å (the distance between points "1" and "2"). On the basis of lattice parameters of 5.42 and 5.13 Å for the CeO_2 and YSZ, respectively, the lattice misfit, F, associated with this configuration can be calculated to be −0.6% following:

$$F = \frac{2[na_{CeO_2} - ma_{YSZ}]}{[na_{CeO_2} + ma_{YSZ}]}$$

where a_{CeO_2} and a_{YSZ} are the lattice parameters of the overlying CeO_2 lattice and YSZ substrate, respectively, and n and m are the number of spacings between coincident sites for the CeO_2 and YSZ, respectively. At the midpoint between "1" and "2", the lattices are misaligned. Clearly, the driving force for the evolution of such a commensurate relationship is the reduction in strain energy. Specifically, if the two lattices were to remain completely coherent ($m = n$) across the region, the two lattices would have to be strained to accommodate the full +5.5% misfit.

Dmowski et al.,[12] who studied the structure of ultrathin CeO_2 overlayers (10−40 Å) on single crystals of YSZ(111), (110), and (100), found that CeO_2 formed epitaxial thin films orientationally matched with the substrate. They also found that the

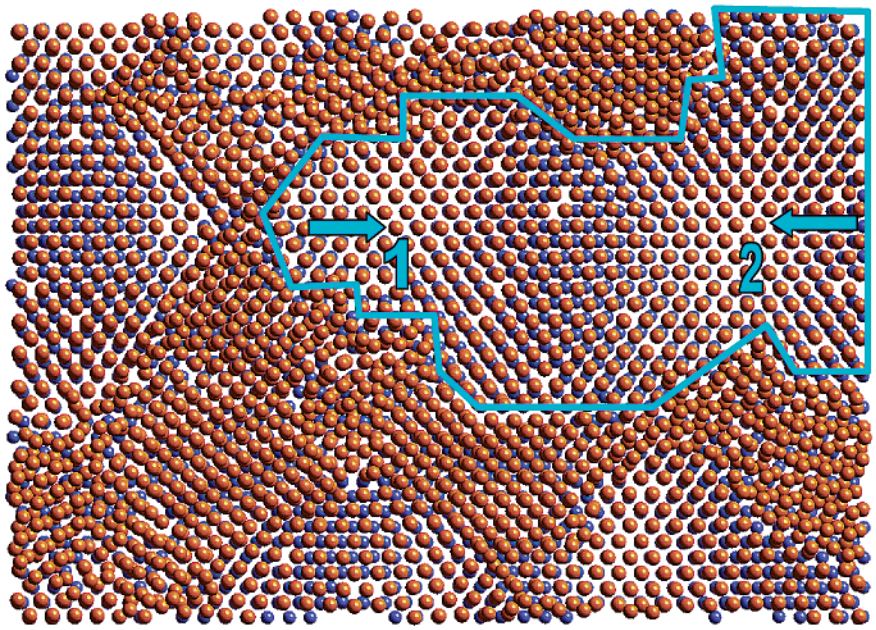

Figure 8. Sphere model representation of a thin slice cut parallel with the interfacial plane through the CeO_2 thin film (Figure 6a; Ce sublattice only) together with a corresponding slice (cation (Zr,Y) sublattice only) cut through the underlying YSZ substrate. A plan view of the system is depicted to illustrate regions of alignment and interconnecting regions of misalignment between the CeO_2 thin film and underlying YSZ substrate. Cerium is colored yellow, and zirconium and yttrium are colored blue.

YSZ lattice parameter was higher than that expected for a 9.5% yttrium-doped zirconia (5.13 Å). Moreover, the authors suggest that there is some inhomogeneity in the YSZ crystal, which results in a change in lattice parameter as a function of depth.

In this present study, the calculated lattice parameter for the YSZ *interfacial* layer is 5.37 Å, which compares with a bulk value of 5.106 Å for the parent oxide. Moreover, this value for the interfacial YSZ lattice parameter is closer to that of the overlying CeO_2 thin film, which is calculated from the RDF data to be 5.44 Å; the lattice parameter for the CeO_2 parent oxide is 5.42 Å. We suggest that the underlying YSZ support relaxes significantly to improve the interaction across the interface and helps minimize the strain gradient as one traverses the interface. In addition, in the top two layers of the CeO_2 thin film, smaller values for the lattice parameter are identified, as compared with bulk values, indicating low coordination of ions comprising these layers.

The Dipolar CeO_2(100) Surface. It is surprising to observe that the simulation generated crystallites exposing CeO_2(100) because this surface is considered unstable because of the dipole generated perpendicular to it.[34] However, while such polar surfaces were assumed not to exist experimentally previously, recent studies have identified that dipolar surfaces can be stabilized via substantial surface reconstruction[35,36] as predicted theoretically by Tasker.[34] In particular, it was shown experimentally, for CeO_2 supported on $SrTiO_3$, that a CeO_2(001) surface can be fabricated with 0.5 monolayers of oxygen terminating the CeO_2(100) surface.[37,38] Nörenberg and Harding, who studied the surface structure of CeO_2(001) single crystals using scanning tunneling microscopy, observed a $0.5\sqrt{2}(3 \times 2)$R45 reconstruction of the surface.[5] The authors suggest that a polar surface is avoided by surface reconstruction with oxygen in the topmost layer.

For the model CeO_2/YSZ(110) system considered in this present study, the surface of a particular CeO_2(100) grain, shown in Figure 9, can be seen to be highly defective in accord with experiment. Specifically, the two surface layers are incomplete with surface oxygen ions contracting into the surface.

It has been shown, theoretically, that the (dipolar) CeO_2(001) surface is less stable[39] than either the (111) or the (110) surfaces, which are not associated with a perpendicular dipole. Because this (001) surface is less stable, it is likely to be inherently more reactive and consequently more important with respect to the catalytic properties of the system.

Discussion

In this study, we have employed a simulated amorphization and recrystallization strategy to explore structures supported on a substrate. In particular, we have used the simulation code, DL_POLY, that performs simulations using three-dimensional periodic boundary conditions, to simulate thin films, which are essentially a two-dimensional problem. While two-dimensional periodic surface codes are available,[40] the reason for using DL_POLY is that it offers a considerable speed advantage for our particular simulations. In particular, the vector, introduced perpendicular to the surface to generate the vacuum above the thin film, is our smallest vector, which facilitates a very efficient 3D summation. Many simulations of surfaces performed using 3D codes are inefficient due to the large sampling of reciprocal lattice vectors perpendicular to the surface in the Ewald summation as compared with the other two directions.

Previous studies have been performed to ensure consistency between the two (2D versus 3D) approaches. Specifically, the models generated by the two codes exhibited no appreciable

(34) Tasker, P. W. *J. Phys. C* **1979**, *12*, 4977.
(35) Oliver, P. M.; Watson, G. W.; Parker, S. C. *Phys. Rev. B* **1995**, *52*, 5323.
(36) Noguera, C. *J. Phys.: Condens. Matter* **2000**, *12*, R367.
(37) Herman, G. S. *Phys. Rev. B* **1999**, *59*, 14899.
(38) Herman, G. S. *Surf. Sci.* **1999**, *437*, 207.
(39) Conesa, J. C. *Surf. Sci.* **1995**, *339*, 337.
(40) Gay, D. H.; Rohl, A. L. *J. Chem. Soc., Faraday Trans.* **1995**, *91*, 925.

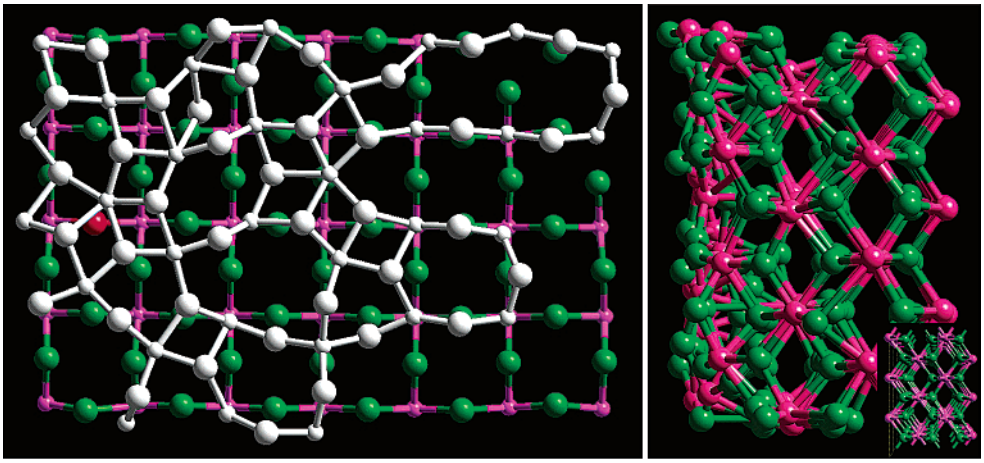

Figure 9. Graphical representation of the surface of a $CeO_2(100)$ nanocrystallite. To the left of the figure, a plan view is presented, and to the right, a side view is depicted. The latter includes a small inset, which depicts a side view of the perfect lattice. For the plan view, the defective nature of the surface ions (colored white; cerium are the smaller white spheres and oxygen the larger spheres) is shown. Cerium is colored pink, and oxygen is colored green.

differences with respect to relative stabilities (thin film energies) and structural features,[29] indicating that the application of three-dimensional periodic boundary conditions with a void to represent the free surface was a valid approach. Details of the simulations performed using two-dimensional periodicity (exploiting the Parry method) and three-dimensional periodicity (Ewald summation) can be found in refs 9 and 11, respectively.

In a previous study,[17] we suggested that CeO_2 thin films, which expose (111) surfaces, could be generated when supported on a YSZ(111) substrate. However, as compared with the CeO_2-(110) surface, the $CeO_2(111)$ surface has been shown to be more stable and less reactive.[4] It is therefore desirable to identify mechanisms for generating the (more reactive) $CeO_2(110)$ surface. Previous studies have shown that the substrate can be exploited to act as a template in directing the structure of a thin film deposited thereon.[41] Accordingly, it is pertinent to suggest, and indeed the impetus underlying this present study, that the $CeO_2(110)$ surface might be exposed if a thin film of CeO_2 is supported on YSZ(110); both materials exhibit a fluorite structure.

The results from this study demonstrate clearly that the YSZ acts as a template in directing the exposure of the $CeO_2(110)$ at the surface of the thin film. For example, supporting a CeO_2 thin film on YSZ(111) resulted in CeO_2 thin films exposing (111) surfaces,[17] while on a YSZ(110) surface, $CeO_2(110)$ surfaces are exposed. Remarkably, for the latter, the CeO_2 exposed also the highly reactive and dipolar $CeO_2(100)$ surface.

We suggest that the structure (surface exposed) and associated misfit between the CeO_2 thin film and underlying YSZ are, in part, responsible for the exposure of the $CeO_2(110)$ and dipolar $CeO_2(100)$ surfaces. For example, with regards to the structure, it is desirable for the overlying thin film to adopt the same orientation as that expressed by the substrate, as this behavior maximizes favorable interactions across the interfacial region. In particular, ions comprising the CeO_2 thin film lie in registry with respect to the underlying substrate (Figure 8, top right). However, on the basis of the 5.5% misfit associated with the CeO_2/YSZ system, the strain energy terms associated with maintaining such registry across the entire interfacial area are prohibitive and cannot be maintained. Accordingly, within the $CeO_2(111)$/YSZ(111) system, dislocations were observed to have evolved to help alleviate the misfit. Conversely, in this present study, grain boundaries, which separate the various nanocrystallites exposing (110) and (100) facets at the surface, enable the overlying CeO_2 to accommodate the strain associated with the system.[42]

Clearly, additional competing factors may contribute to the observed behavior. These may include, for example, nucleation and growth (as the thin film recrystallizes), the nature or surface roughness of the substrate, and thin film (critical) thicknesses.[43] Accordingly, further work needs to be undertaken to secure a definitive understanding of the behavior.

The study demonstrates why and how intrinsically unstable (but desirable), highly reactive surfaces can be expressed. In addition, it offers the possibility of "fine-tuning" the substrate to optimize the amount of reactive surface, providing a prediction for materials chemistry.

Conclusions

A simulated amorphization and recrystallization strategy has been employed to observe the evolution of structural modifications that arise in the CeO_2/YSZ(110) system. The rationale underlying this study was to generate models, which include the exposure of the more reactive $CeO_2(110)$ surface by supporting a CeO_2 thin film on YSZ(110); a previous study in which CeO_2 was supported on YSZ(111) resulted in $CeO_2(111)$ films.[17] Surprisingly, when supported on YSZ(110), the CeO_2 thin film evolved into a polycrystalline structure comprising (111), (110), and (100) crystallites separated by many grain boundaries and grain junctions. The exposure of the (100) is significant in that it is dipolar and consequently potentially more reactive and important catalytically as compared with either the (111) or the (110). Moreover, the surface of the $CeO_2(100)$ was observed to be highly defective with low coordinative saturation of the surface ions, which may influence their lability or alternatively the lability of neighboring ions with implications for the OSC of the material. The atomistic models generated in this study are therefore important in helping rationalize the active sites that are present on the surface of a catalytic material.

(41) Sayle, D. C.; Watson, G. W. *J. Phys. Chem. B* **2002**, *106*, 3778.

(42) Schiotz, J.; Di Tolla, F. D.; Jacobsen, K. W. *Nature* **1998**, *391*, 561.

(43) Dong, L.; Schnitker, J.; Smith, R. W.; Srolovitz, D. J. *J. Appl. Phys.* **1998**, *83*, 217.

Future studies will focus on addressing the binding energies (reactivity) of the surface oxygen ions and exploring the migration (mobility) of oxygen ions within the supported CeO_2 lattice.

Acknowledgment. We acknowledge funding for a 20 processor Compaq SC cluster, located at the Rutherford Appleton Laboratory, which was purchased and supported with funding from the JREI (JR99BAPAEQ) and Compaq; Enterprise Ireland for a Basic Research Grant (SC/2001/233); CCP5 for a travel grant; and John H. Harding and Steve C. Parker for useful discussions.

JA020657F